



Modeling and simulation of biogas-fueled power system

Mohammed Saeed, Samaa Fawzy & Magdi El-Saadawi

To cite this article: Mohammed Saeed, Samaa Fawzy & Magdi El-Saadawi (2019) Modeling and simulation of biogas-fueled power system, International Journal of Green Energy, 16:2, 125-151, DOI: [10.1080/15435075.2018.1549997](https://doi.org/10.1080/15435075.2018.1549997)

To link to this article: <https://doi.org/10.1080/15435075.2018.1549997>



Published online: 24 Nov 2018.



Submit your article to this journal 



Article views: 114



View Crossmark data 



Modeling and simulation of biogas-fueled power system

Mohammed Saeed, Samaa Fawzy, and Magdi El-Saadawi

Department of Electrical Engineering, Faculty of Engineering, Mansoura University, Mansoura, Egypt

ABSTRACT

The main objective of this paper is to develop a complete model that fully simulate a biogas-fueled power plant which can be used to supply a rural farm with sufficient electricity. The reactor is fed with animal manure of the farm. The proposed model consists of three main parts; a biogas reactor, a microturbine (MT) coupled to a permanent magnet synchronous generator, and a storage system. The model describes the dynamics of an MT and it is suitable for both steady state and transient simulation and analysis. The volume of biogas output delivered from the Anaerobic Digester depends on the reactor volume, reactor temperature, and animal manure type. The storage system is used to store the excess value of biogas if any. It is composed of two parts: a comparator and a storage tank. The comparator compares the volume of biogas produced by the reactor with that needed to supply the load. An adaptive controller is developed to withstand the system against any transient condition such as suddenly load increase/decrease. The proposed model is implemented for chemical and physical behaviors of the biogas production process, as well as for different variables of MT-generator operations. The model is implemented in Matlab/Simulink environment and tested under different operating conditions in both steady state and transient status to study the impacts of different variables on the system output. The output results prove its applicability and effectiveness under different operating conditions.

ARTICLE HISTORY

Received 23 May 2018

Accepted 15 November 2018

KEYWORDS

Biomass; anaerobic digestion; microturbine; modeling; simulation

1. Introduction

The use of renewable energy sources is becoming increasingly necessary, to meet the growing demand for energy. Biomass is the most common form of renewable energy, widely used in the third world (McKendry 2002c). The use of biomass to provide energy has been fundamental to the development of civilization. In recent times, pressures on the global environment have led to an increased use of renewable energy sources, rather than fossil fuels (McKendry 2002d). Biomass is the plant material derived from the reaction between CO₂ in the air, water and sunlight, via photosynthesis, to produce carbohydrates that form the building blocks of biomass (Capareda 2013b). It includes all plant and animal living matter. The most commonly form of biomass resources is plant biomass resulting from agriculture food production. Other sources of biomass include forestry resource and residue and animal manure from confined animal production operations (Wellinger, Murphy, and Baxter 2013b). As an energy resource, there are several advantages in using biomass as a fuel energy; it provides an efficient source of low sulfur fuel, it is a relatively cheap source of energy, and it reduces environmental risks (Saroj 2012b).

Bioenergy derived from biomass may play a significant role in future energy systems due to its renewability and sustainability. The wide distribution of biomass provides rich sources of raw materials, while the significant development in bioenergy conversion technology has improved its competitiveness. Bioenergy,

which is used to produce biofuel, heat, and electricity, may be generated via various routes such as thermo-chemical, biological, and bio-electrochemical processes. Bioenergy systems should be optimized to ensure their sustainability, maximize their efficiency, and minimize costs.

The bioreactor is a critical unit in the microbial conversion process, since it provides a suitable, stable place for microbial growth and metabolism by controlling the operating conditions. The performance of bioreactors is greatly influenced by many other factors, such as the bioreactor's structure and size, mixing and transfer characteristics, and means of feed introduction and product removal. There are complex multiphase flow patterns that exist in bioreactors which can vary the heat and mass transfer characteristics in the bioreactors and affect the microbial conversion processes (Liao et al. 2018b).

There are different ways to convert biomass resources into useful energy. In some ways, the conversion process is dependent on specific properties of the biomass, such as moisture and ash content. On other ways, the conversion process is affected by the energy content of the biomass resource. One important type of these conversion processes is the Anaerobic Digestion (AD) in which the biomass sources are used to produce biogas (Hagos et al. 2017b). During fermentation process, many types of biomass can be used in anaerobic digesters such as, crop residues, animal manure, and food waste (Neshata et al. 2017b; Zhang, Hu, and Lee 2016b). Many researches have discussed different aspects of biogas production, processing and utilization. Hagos et al. (2017b;

Neshata et al. 2017b; Zhang, Hu, and Lee 2016b) presented research updates on biogas production from AD processes. Hagos et al. (2017b) presented an assessment of the current status of biogas production process, and the challenges and perspectives for further improvements in China. Neshata et al. (2017b) presented a review on anaerobic co-digestion of animal manure and lignocellulosic feedstock for biogas production. Zhang, Hu, and Lee (2016b) summarized the new trends and technologies in biogas production from AD process.

Several methods were used for modeling and simulating different components of biogas power plants (Abdollahi and Vahedi 2005b; Al-Hinai and Feliachi 2002b; Asgharian and Noroozian 2016b; Barsali et al. 2015b; Corigliano, Florio, and Fragiocomo 2012b; De Lorenzo et al. 2016b; Duan, Bournazou, and Kravaris 2017b; Guda 2005b; Guda, Wang, and Nehrir 2006b; Haugen, Bakke, and Lie 2012b; Husain 1998b; Khorshidi, Zolfaghari, and Akhavan 2014b; Manjusha and Beevi 2016b; Pathmasiri, Haugen, and Gunawardena 2013b; Rathnasiri 2016b; Shi et al. 2014b; Ting Chen et al. 2017b; Weinrich and Nelles 2015b). Husain (1998b) presented a review of steady state and dynamic models of the kinetics of AD. A detailed description of the digestion process with kinetic parameters independent of the type of waste was delivered. Pathmasiri, Haugen, and Gunawardena (2013b) developed a Simulink model for biogas reactor using only dairy manure. In this study a modified Hill's model simulated in Matlab environment using Euler method and ode solver were applied to obtain the change of methane gas production with time. Haugen, Bakke, and Lie (2012b) presented a dynamic model of AD biorreactor using dairy manure to analyze both steady state and dynamic operational statuses. Shi et al. (2014b) introduced a dynamic mathematical model based on IWA AD Model No. 1 (ADM1) to predict the methane yield and the pH value during anaerobic co-digestion of dairy manure and spent mushroom substrate under different hydraulic retention times. Different model structures to simulate the characteristic process variables of the AD of sugar beet, maize, and grain silage were compared in Weinrich and Nelles (2015b). Rathnasiri (2016b) investigated the effect of recycling sludge and stability of pilot scale AD plant treating organic fraction of source separated food waste. ADM1 was applied for modeling and simulation of continuous stirred tank anaerobic reactor including recycling (Manjusha and Beevi 2016b). Chen et al. (2017b) presented a quantitative Fuzzy evaluation of environ-economic benefits of AD of food waste. The evaluation was conducted on an operational project in China. Finally, a two-stage model based on two-step mass-balance model was developed in Duan, Bournazou, and Kravaris (2017b). The model incorporated acidogenesis in the first stage and mainly methanogenesis in the second one. A comparison between the operation of both two-stage and one-stage processes was presented.

On the other hand, modeling and simulation of an MT system was presented in many papers (Abdollahi and Vahedi 2005b; Al-Hinai and Feliachi 2002b; Asgharian and Noroozian 2016b; Guda 2005b; Guda, Wang, and Nehrir 2006b; Khorshidi, Zolfaghari, and Akhavan 2014b). A set of mathematical equations were used to model an MT system (Guda 2005b; Guda, Wang, and Nehrir 2006b). The developed model was capable of simulating the dynamic behavior of MT generation system and indicating its ability to meet electric

load requirements. Dynamic modeling and simulation of MT systems were presented in Abdollahi and Vahedi (2005b; Al-Hinai and Feliachi 2002b; Asgharian and Noroozian 2016b; Khorshidi, Zolfaghari, and Akhavan 2014b). The models were mainly composed of a gas turbine engine, a permanent magnet generator and power electronics interfacing.

Barsali et al. (2015b) presented an externally fired micro gas turbine supplying 70 kW of electricity as well as 200–250 kW of useful heat. The paper presented the mathematical model for the physical and chemical behaviors of both biomass combustion process, and heat transfer mechanisms to assess the biomass power plant using micro gas turbine operating variables in both steady state and transient operating conditions. Corigliano, Florio, and Fragiocomo (2012b) formalized a zero-dimensional stationary mathematical model for high temperature solid oxide and molten carbonate fuel cells fed by biogas. The model was implemented in MATLAB computing environment. Through the calculation tool it was possible to analyze the biogas reforming process. De Lorenzo et al. (2016b) formulated a numerical model of a Solid Oxide Fuel Cell system with Ni-Fe/CGO electrocatalyst anode protective layer directly fed by dry biogas, in cogenerate arrangement and with anode exhaust gas recirculation is formulated. Galvagno et al. (2013b) investigated biogas reforming processes (steam reforming, auto thermal reforming and partial oxidation). A mathematical model was developed, and an experimental validation was made in order to confirm model results.

The main contributions of this paper are the developing complete detailed model that fully simulate a biogas-fueled power plant. The proposed model is composed of three individual models represent a biogas reactor, a microturbine (MT)-generation system and a storage system. Each model can be implemented individually or collectively to simulate the biogas power plant. An adaptive controller was developed to withstand the plant against any transient condition.

The rest of this paper is organized as follows. Section 2 explains the AD process. A detailed mathematical modeling for biogas power plant components is introduced in Section 3. Section 4 discusses the testing and validation of the proposed model at different operation scenarios. The simulation results of the proposed model under different operation conditions are analyzed in Section 5. Finally, the paper is concluded in Section 6.

2. Anaerobic digestion process

AD is a biochemical conversion process carried out by various microorganisms in which the biomass organic material is converted into organic acids, which in turn are converted into methane gas with carbon dioxide as the other byproduct. The process takes place under very strict anaerobic conditions (no oxygen). Anaerobic treatment typically removes Chemical Oxygen Demand (COD) by boiling down the organics to methane. Consequently, the COD of the methane produced in an anaerobic system is often tantamount to the amount of COD removed. The entire process takes place in four clearly defined process and includes the following four distinct events.

2.1. Hydrolysis

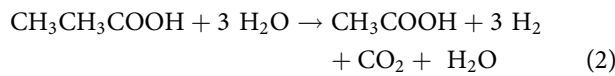
Hydrolysis is the process of converting insoluble complex biomass into soluble compounds by the action of extracellular enzymes of hydrolytic bacteria. These bacteria are the first set of microorganisms that breaks down the biomass into simpler compounds. Carbohydrates, fats and proteins are converted into sugars, fatty acids, and ammonia acids. At the end of hydrolysis process, the complex organics are converted into simpler organics, mostly volatile fatty acids (Pathmasiri, Haugen, and Gunawardena 2013b).

2.2. Acidogenesis

The second step is the conversion of soluble organics from hydrolysis into short-chain fatty acids and alcohols. Most acids are converted into acetic acid via the step of conversion into acetic acid. Other organic acids are also produced, such as propionic, butyric, valeric and others. At this stage, hydrogen is produced by the fermentation of glucose. The microbes responsible for this process are called "acid formers" and are composed of homoacetogenic bacteria and some facultative bacteria. In this step, acetic acids and water are converted into carbon dioxide and hydrogen.

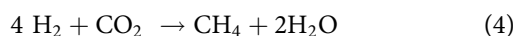
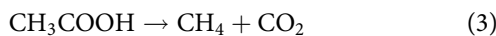
2.3. Acetogenesis

This step represents the widespread production of acetic acid by hydrogenation. Acetic acid may also be formed by the dehydrogenation process. During the AD process, acetic acids are the most abundant organic acids produced, among many other fatty acids (Husain 1998b; Pathmasiri, Haugen, and Gunawardena 2013b). The following equations represent the production of acetate by hydrogenation and by dehydrogenation, respectively:



2.4. Methanogenesis

The final step in the AD is the conversion of organic acids into methane by the action of methane-producing microbes. The methanogenesis process is divided into two stages. The first stage is the conversion of acetic acid into methane, which comprises about 70% of the process reactions. The second stage is the conversion of hydrogen into methane utilizing the carbon dioxide produced during the process, which comprises the remaining 30% of the process reactions. The following equations represent acetotrophic coming from acetic acid and hydrogenotrophic coming from H_2 , respectively:



The four stages of the AD process are shown in Figure 1.

3. Mathematical modeling

The proposed model consists of three main parts; biogas reactor, MT coupled to permanent magnet synchronous generator, and storage system. This section presents mathematical Modeling and simulation for these parts.

3.1. Modeling of biogas reactor

The reactor mathematical model can be represented by a set of differential equations that characterize the dynamic behavior of the four pre-mentioned stages in a constant volume AD bioreactor. The volume of output methane delivered from this model depends on the reactor volume, reactor temperature, and the type of animal manure.

3.1.1. Hydrolysis modeling

Hydrolysis process is the first stage in AD process. This process can be represented as the rate of change of biodegradable volatile solids (BVS) concentration in the reactor during the AD process. The process depends on the type of feed material, the feed flow rate, effective reactor volume and reactor temperature. The following equation represents the hydrolysis process (Haugen, Bakke, and Lie 2012b):

$$\frac{d(\text{Sb})}{dt} = (\text{Sb}_{in} - \text{Sb}) \left(\frac{F_{feed}}{V} \right) + \frac{\mu_m K_1 X_{acid}}{\frac{K_s}{\text{Sb}} + 1} \quad (5)$$

where

Sb is the concentration of biodegradable volatile solids in the reactor (kg/m^3),

Sb_{in} is the concentration of biodegradable volatile solids in the reactor feed (kg/m^3),

F_{feed} is the feed flow rate (m^3/day),

V is the effective reactor volume (m^3),

K_1 is the yield factor estimated using experimental data as given in (Haugen, Bakke, and Lie 2012b),

X_{acid} is the concentration of acidogens (kg/m^3),

K_s is the Monod half-velocity constant for acidogens (kg/m^3),

μ_m is the maximum growth rate for acidogens (d^{-1}),

X_{acid} is the concentration of acidogens (kg/m^3), and

X_{meth} is the concentration of methanogens (kg/m^3).

The maximum growth rate for methanogens can be expressed as a function of temperature dependence of reaction rates using the following empirical formula (Haugen, Bakke, and Lie 2012b; Pathmasiri, Haugen, and Gunawardena 2013b):

$$\mu_m(T_{react}) = \mu_{mc}(T_{react}) = 0.013 \cdot T_{react} - 0.129 \quad (6)$$

where μ_{mc} is the maximum growth rate for methanogens (d^{-1}) and T_{react} is the reactor temperature ($^\circ\text{C}$). The Simulink model represents the hydrolysis process is shown in Figure 2.

3.1.2. Acidogenesis modeling

The acidogenesis stage represents the rate of change of volatile fatty acid concentration during the fermentation process. The process depends on the concentration of total volatile fatty acids in the reactor (type of feed material), the feed flow rate, effective reactor volume, and reactor temperature. The following equation

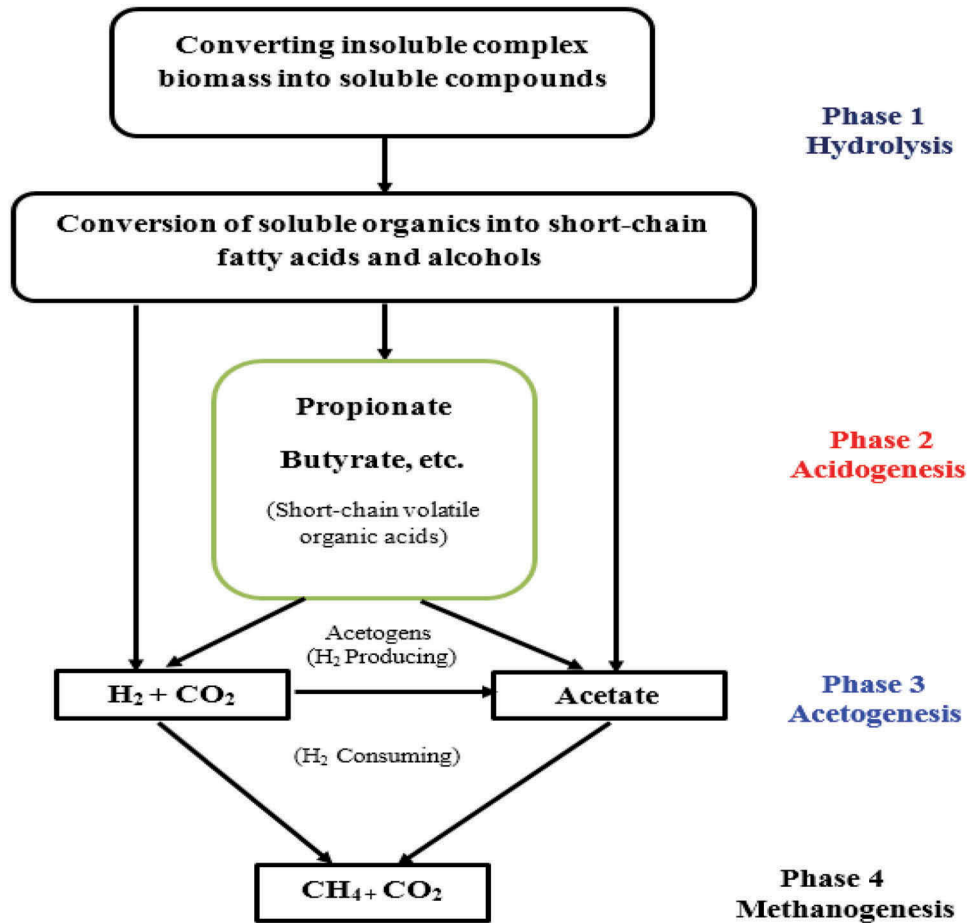


Figure 1. A schematic diagram of the four stages of AD process.

represents the acidogenesis process (Haugen, Bakke, and Lie 2012b):

$$\frac{d(Sv)}{dt} = (Sv_{in} - Sv) \cdot \left(\frac{F_{feed}}{V} \right) + \frac{\mu_m K_2 \cdot X_{acid}}{\frac{K_s}{Sb} + 1} - \frac{\mu_{mc} K_3 \cdot X_{meth}}{\frac{K_{sc}}{Sv} + 1} \quad (7)$$

where

Sv is the concentration of total volatile fatty acids in the reactor (kg/m^3),

Sv_{in} is the concentration of total volatile fatty acids in the reactor feed (kg/m^3),

K_2 is the yield factor estimated using experimental data,

K_3 is the yield factor related to growth rate of methane gas, and

K_{sc} Monod half-velocity constant for methanogens (kg/m^3).

The Simulink model represents the acidogenesis process, as shown in Figure 3.

3.1.3. Acetogenesis modeling

The third stage of AD process represents acidogenesis process. This process depends on both concentration of acidogens, type of feed material, feed flow rate, effective reactor volume and reactor temperature. The following equation represents the acetogenesis process (Haugen, Bakke, and Lie 2012b; Pathmasiri, Haugen, and Gunawardena 2013b):

$$\frac{d(X_{acid})}{dt} = \left[\frac{\mu_m}{\frac{K_s}{Sb} + 1} - K_d - \left(\frac{F_{feed}/b}{V} \right) \right] \cdot X_{acid} \quad (8)$$

where b is the retention time factor estimated using experimental data (Haugen, Bakke, and Lie 2012b) and K_d is the specific death rate of acidogens (d^{-1}).

The Simulink model in Figure 4 represents this process.

3.1.4. Methanogenesis modeling

Methanogenesis stage determines the concentration of methanogens that are used to produce methane. This stage is represented by (9) (Haugen, Bakke, and Lie 2012b; Pathmasiri, Haugen, and Gunawardena 2013b). The process depends on retention time, the feed flow rate, effective reactor volume, and reactor temperature:

$$\frac{d(X_{meth})}{dt} = \left[\frac{\mu_{mc}}{\frac{K_{sc}}{Sv} + 1} - K_{dc} - \left(\frac{F_{feed}/b}{V} \right) \right] \cdot X_{meth} \quad (9)$$

where K_{dc} is the specific death rate of a methanogens (d^{-1}) and X_{meth} is the concentration of methanogens (kg/m^3).

Figure 5 illustrates the Simulink model of methanogenesis process.

The amount of methane output from reactor is determined as follows:

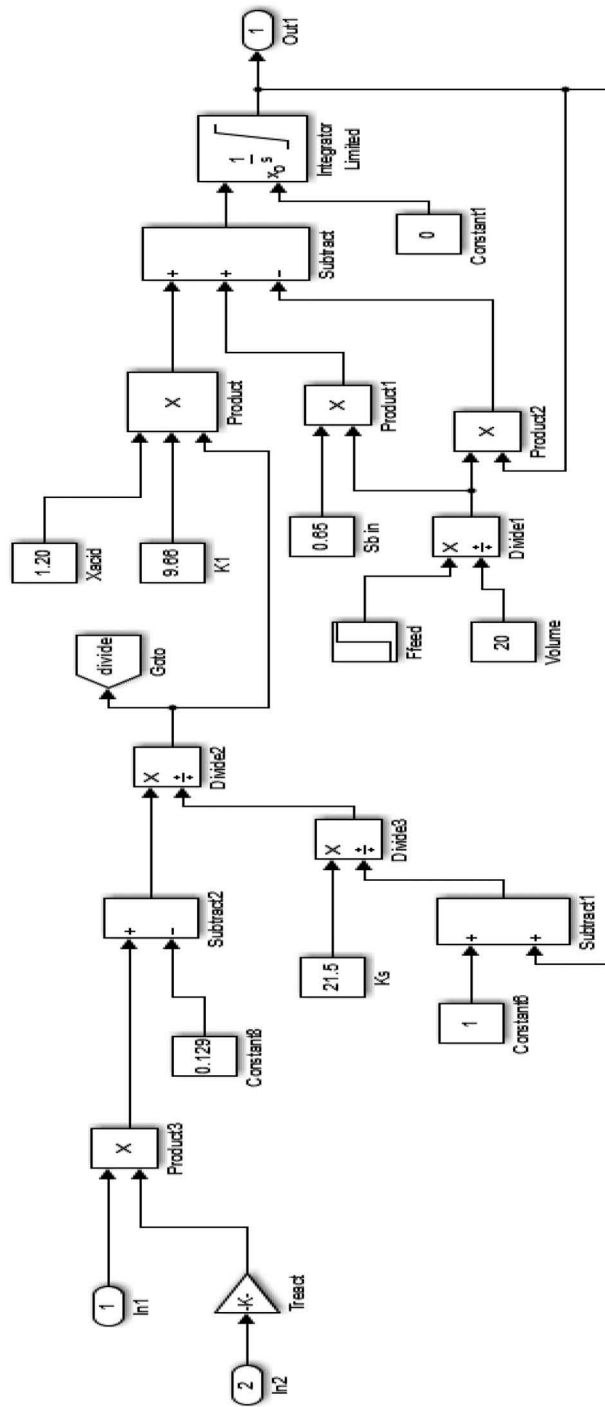


Figure 2. Simulink model for hydrolysis process.

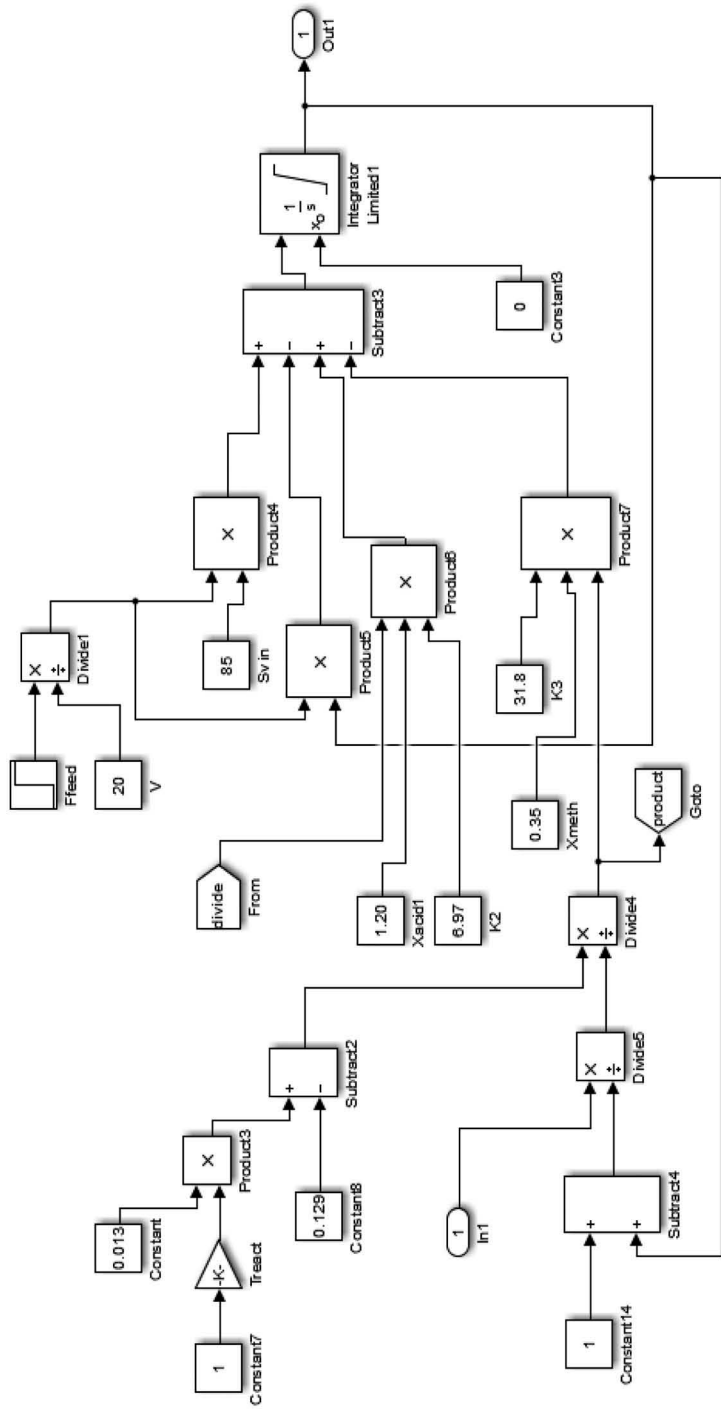


Figure 3. Simulink model for acidogenesis process.

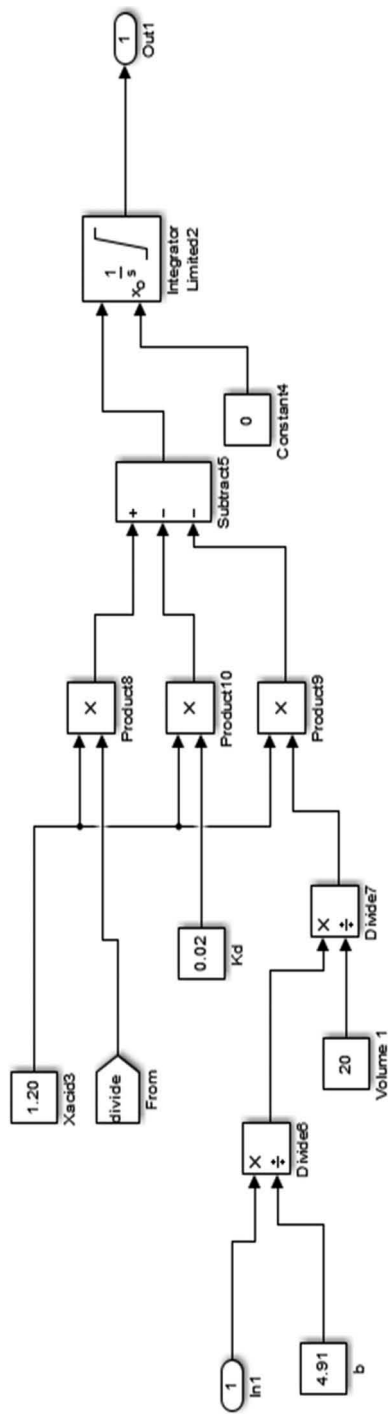


Figure 4. Simulink model represents acidogenesis process.

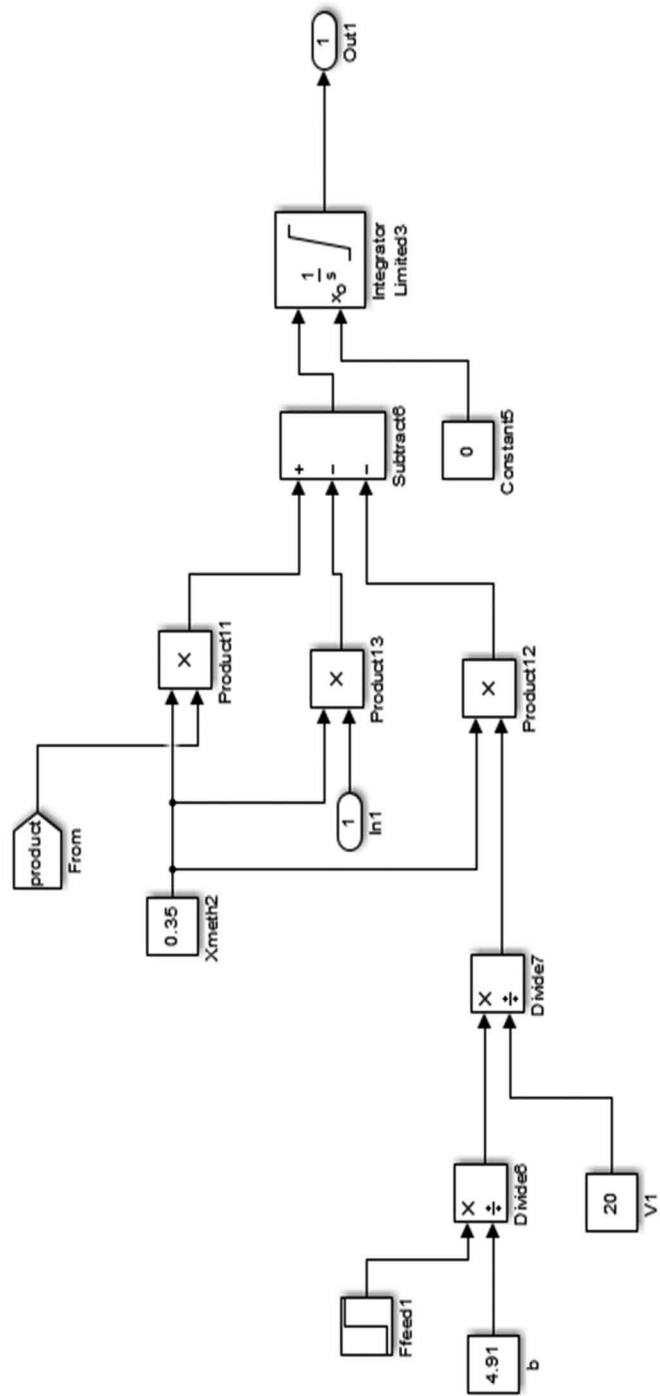


Figure 5. Simulink model of methanogenesis process.



$$F_{\text{meth}} = V \cdot \frac{\mu_{\text{mc}}}{\frac{K_{\text{sc}}}{Sv} + 1} \cdot K_4 \cdot X_{\text{meth}} \quad (10)$$

where K_4 is a factor related to the methane gas flow and estimated from experimental data (Haugen, Bakke, and Lie 2012b).

A Simulink model for this equation is shown in Figure 6.

3.1.5. Reactor Simulink model

Figure 7 shows the complete Simulink model for the previous four stages of AD process represented by Equations (5)–(10).

3.2. Modeling and control of a microturbine-generation system

MTs are small gas turbines burns gaseous or liquid fuels to produce high energy gas stream that runs an electrical generator. In the following subsections; a brief description of MT components and its principle of working is presented. A proposed Simulink model for an MT-generation system is then derived and finally a Simulink model for PMSG driven by MT is presented.

3.2.1. Principles of microturbine working

MT produces electrical power via a high-speed generator directly driven by the turbo-compressor shaft. Small gas turbines benefit in particular when the gearbox that reduces the shaft speed to the speed of conventional electrical machines is eliminated, as is the case with the single-shaft designs considered here. The result is a more efficient, compact and reliable machine and the shaft speed is normally above 30,000 rev/min and may exceed 100,000 rev/min. High energy permanent magnets and high yield-strength materials like neodymium-iron-boron or Samarium-cobalt magnets have proved very suitable for high-speed electrical machines (Guda 2005b).

In a PMSG, the dc field winding of the rotor is replaced by a permanent magnet. The PMSG advantages are as follows: elimination of filed copper loss, higher power density, lower rotor inertia, and more robust construction of the rotor. The drawbacks are: loss of flexibility of field flux control and

possible demagnetization. The machine has higher efficiency than an induction machine, but generally its cost is higher.

The basic components of an MT generation system include compressor, turbine, recuperator, and permanent magnet synchronous generator with power electronics interfacing. MT operation is based on Brayton cycle. The choice of whether to use a single-shaft MT or two-shaft type is largely determined by the characteristics of the driven load. If the load speed is constant, as in the case of an electric generator, a single-shaft unit is often specified; an engine specifically designed for electric power generation would make use of a single-shaft configuration. An alternative, however, is the use of a two-shaft engine. If the load needs to be driven with varying speeds, two-shaft engines are advantageous. The inlet air is compressed in a radial compressor. This air is mixed with fuel in the combustor and burned. The hot burning gas is amplified in the turbine to produce rotating mechanical power to rotate the compressor and the electric generator. To increase the overall efficiency, an air-to-gas heat exchanger called recuperator is added. Without a recuperator the overall efficiency of an MT is 15 to 17%, whereas it can be increased to 33 to 37% with an 85% effective recuperator (Duan, Bournazou, and Kravaris 2017b). A schematic diagram of an MT system is illustrated in Figure 8 (Guda 2005b).

3.2.2. Modeling of a microturbine

The proposed model describes the dynamics of an MT and it is suitable for both steady state and transient simulation and analysis. The model includes a governor speed control, temperature control, acceleration control, fuel system control, and compressor-turbine model.

3.2.2.1. Speed control. Speed control is the primary means of control for the MT under partial load conditions. It operates on the speed error formed between a reference speed (one p.u) and the synchronous generator rotor speed. Speed control is usually modeled by using a lead-lag transfer function, or by a PID controller in this paper a lead-lag transfer function used to represent the speed control. A droop governor is a straight proportional speed controller in which the output is

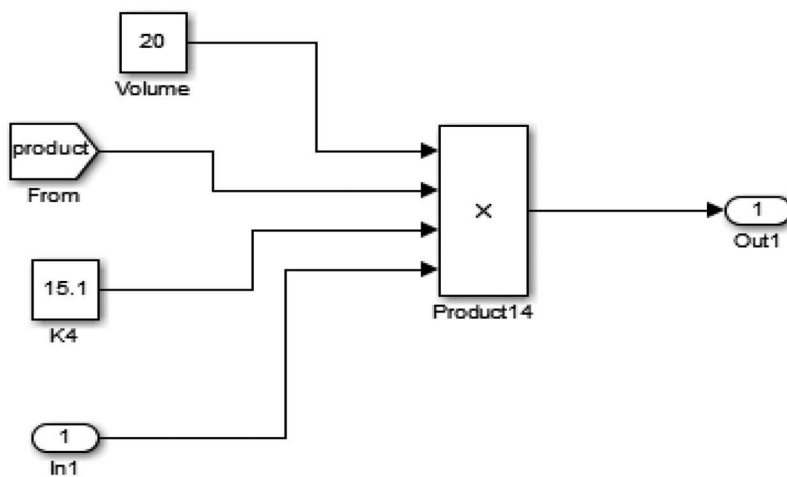


Figure 6. Simulink model represent amount of methane output from reactor.

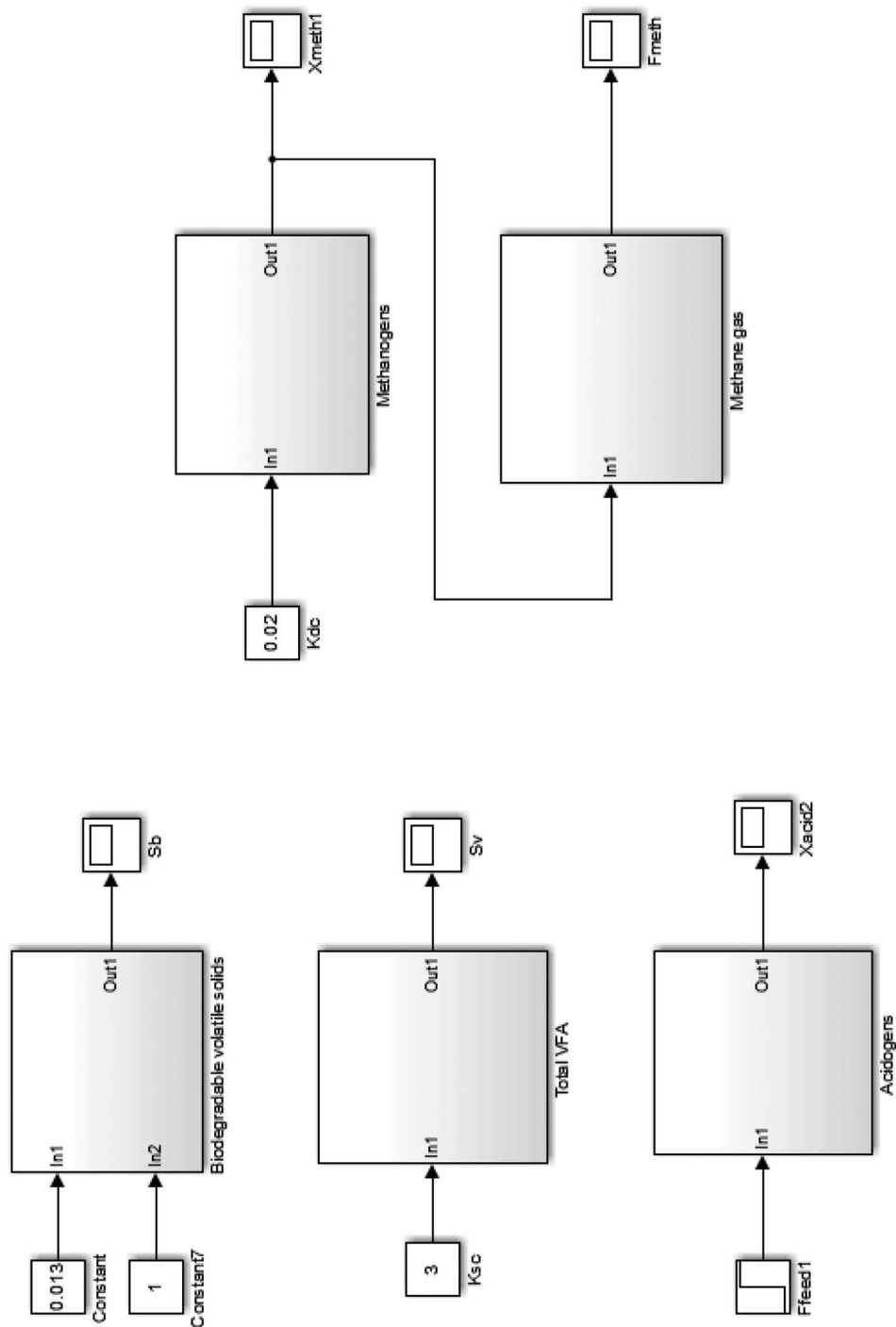


Figure 7. Simulink model of biogas reactor.

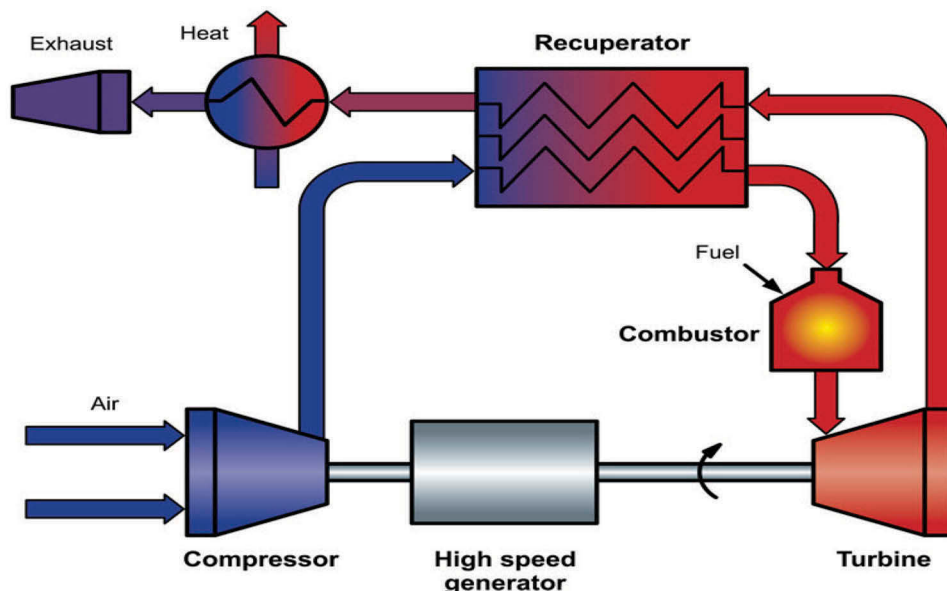


Figure 8. A schematic diagram of an MT system (Guda 2005b).

proportional to the speed error. An isochronous speed controller is a proportional-plus-reset speed controller in which the rate of change of the output is proportional to the speed error. Any increase in the load, leads to a decrease in the speed. **Figure 9** represents a block diagram for this control function (Khorshidi, Zolfaghari, and Akhavan 2014b). In this figure, K is a controller gain, T_1 , T_2 are governor lead and lag time constants, respectively, and Z is a constant representing the governor mode.

3.2.2.2. Temperature control. A temperature controller is employed to restrict the gas turbine output power at a predetermined firing temperature, independent of variations in ambient temperature or fuel characteristics. The fuel, burned in the combustor, produces hot exhaust gases. A series of thermocouples incorporating in radiation shields are used to measure the temperature of these exhaust gases.

The yield from the thermocouple is compared with a reference temperature, which is usually higher than the thermocouple output. This pushes the output of the temperature controller to persist on the maximum limit permitting the control of speed control through the Least Value Gate (LVG). When the thermocouple output exceeds the reference temperature, the difference becomes negative, and the temperature control output decreases. Whenever the signal gets more depression than

the speed controller output, the former value will fall through the LVG to limit the turbine's output. The input to the temperature controller is the exhaust temperature and the output is the temperature control signal to the LVG. **Figure 10** illustrates a block diagram of the temperature controller, where T_t is the temperature controller integration, T_3 , T_4 are time constants associated with radiation shield and thermocouple, respectively, K_1 , K_2 are constants associated with radiation shield and T_5 is a time constant associated with temperature controller.

3.2.2.3. Acceleration control. This type of control is employed primarily during turbine startup to set the rate of the rotor acceleration prior to reaching the operating speed. The output of these control functions is input signals to an LVG. The output of this LVG gate is the lowest of the three inputs which results in the least amount of fuel passed to the compressor-turbine, as revealed by **Figure 11**.

3.2.2.4. Fuel system control. The fuel system consists of a fuel valve and an actuator. The fuel flows from the fuel system actuator through the valve positioner. The valve positioner transfer function is as follows (Guda 2005b):

$$E_1 = \frac{K_v}{T_v s + C} F_d \quad (11)$$

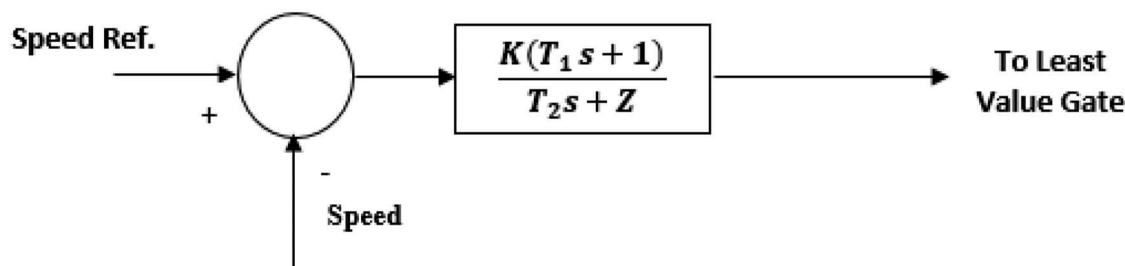


Figure 9. Block diagram represents MT speed control.

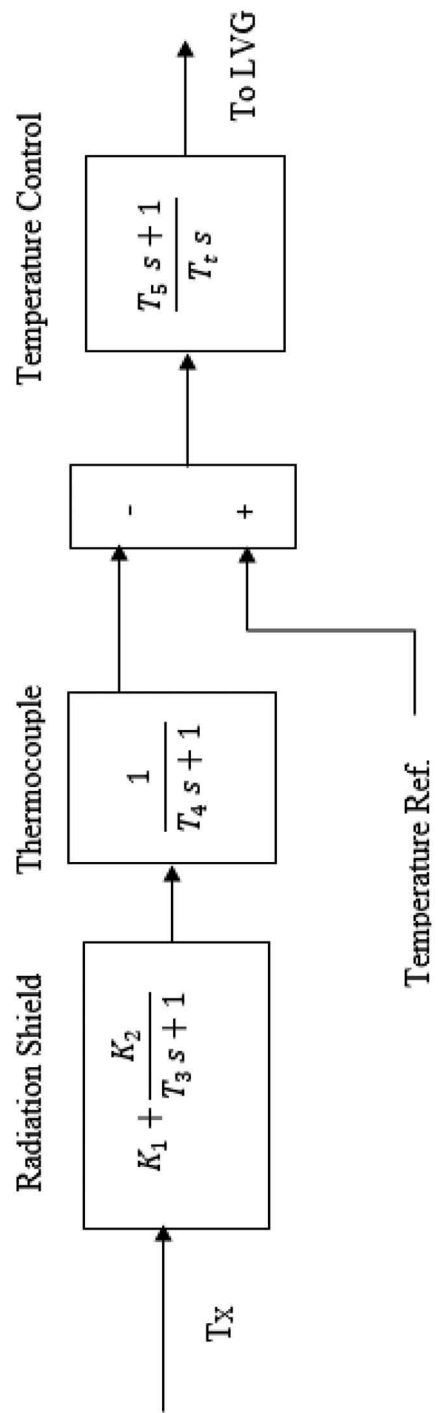


Figure 10. Block diagram of temperature controller.

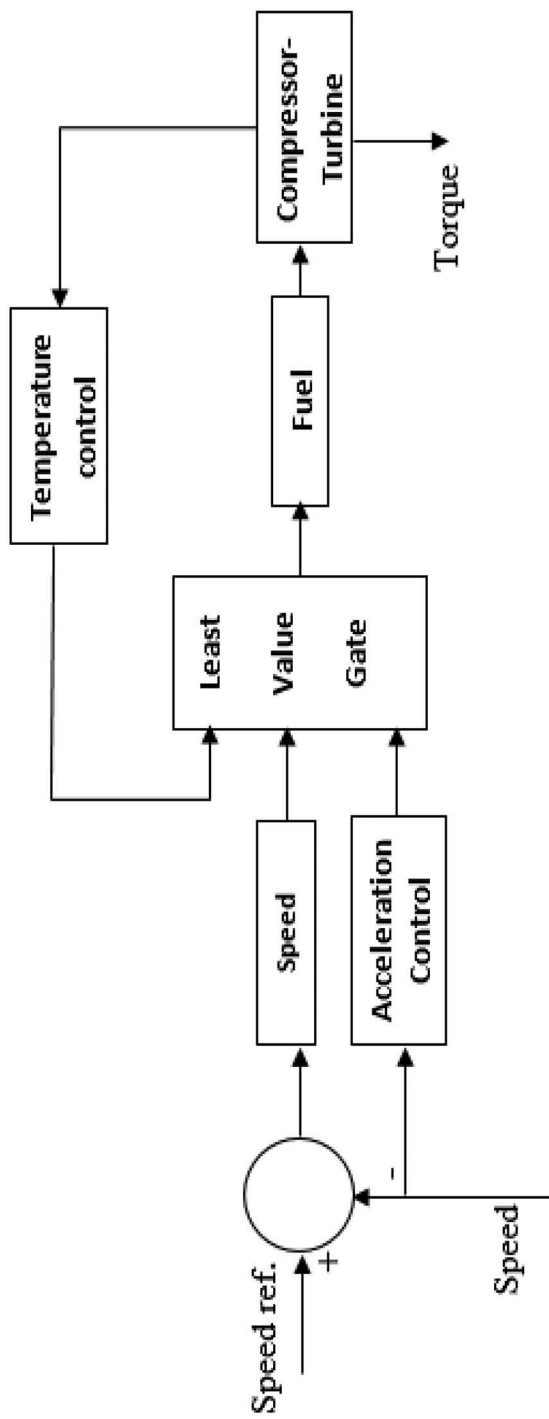


Figure 11. Block diagram of an MT control function.

However, the fuel system actuator transfer function is as follows (Guda 2005b):

$$W_f = \frac{K_f}{T_f S + C} E_1 \quad (12)$$

where

K_v, K_f are valve positioner and fuel system actuator gain, respectively,

T_v, T_f are valve positioner and fuel system actuator time constants, respectively,

F_d, E_1 are input and outputs of the valve positioner, respectively,

C is a constant for transfer function, and

W_f is the fuel demand signal in per unit.

The output of LVG is the least amount of fuel needed for a specific operating point V_{ce} . This output is used as an input to fuel system. Another input to the fuel system is the p.u turbine speed N . The p.u value of V_{ce} is directly proportional to the p.u value of the mechanical power on turbine at steady state. Figure 12 shows the fuel flow control as a function of V_{ce} , where K_3 is the minimum amount of fuel flow at no-load.

3.2.2.5. Compressor-turbine model. The function of the compressor in an MT is to supply air in sufficient quantity to satisfy the requirements of the combustion burners. The compressor increases the pressure of the air received from the air inlet duct, and then, discharges it to the burners at the required magnitude and pressure.

There is a small transport delay T_{CR} , associated with the combustion reaction time, a time lag T_{CD} , associated with the compressor discharge volume and a transport delay T_{TD} , associated with the transportation of gas from the combustion system through the turbine. Figure 13 shows a block diagram of the compressor-turbine model. The equations that describe the compressor-turbine model are shown in Appendix 2.

3.2.2.6. Turbine dynamics. Both the torque and exhaust temperature characteristics of a single-shaft gas turbine is essentially linear with respect to fuel flow and turbine speed. The produced mechanical torque driving the electric generator is presented as follows:

$$T = KH(W_f - 0.23) + 0.5(1 - N) \quad (13)$$

For purposes of MT temperature control, the temperature of the turbine is calculated as follows (Guda 2005b):

$$T_x = T_R - 700(1 - W_f) + 550(1 - N) \quad (14)$$

where KH is a coefficient depends on the enthalpy of the gas stream in the combustion chamber, T_R is the reference temperature, N is the p.u turbine speed and W_f is the p.u fuel demand signal.

The input to this subsystem is the p.u. fuel demand signal W_f and outputs are the p.u. turbine torque. A complete Simulink model represents MT and including all its control systems, as shown in Appendix 3.

3.2.3. Permanent magnet synchronous generator model

In this study, a 4-pole high-speed PMSG with a non-salient rotor model is coupled with the biogas MT to generate ac electricity. A second-order state space model is used to represent both the electrical and mechanical parts of the generator. In this paper the flux established in the stator is assumed to be pure sinusoidal, which implies that electromotive forces are also sinusoidal. In a PMSG, the permanent magnets are glued on the rotor in surface sinusoidal magnet machine, and are mounted inside the rotor in case of an interior magnet synchronous machine. The stator has three phase sinusoidal winding, which creates a synchronously rotating air gap flux. If the machine is rotated by a prime mover, the stator windings generate balanced three-phase sinusoidal voltages. The PMSG configuration can be expressed in dq0 reference frame (for a balanced system the 0-axis quantities are equal to zero) as follows:

$$\frac{d}{dt} i_d = \frac{1}{L_d} V_d - \frac{R}{L_d} i_d + \frac{L_q}{L_d} P W_r i_q \quad (15)$$

$$\frac{d}{dt} i_q = \frac{1}{L_q} V_q - \frac{R}{L_q} i_q - \frac{L_d}{L_q} P W_r i_d - \frac{P W_r}{L_q} \quad (16)$$

Ignoring core loss, $d-q$ axis voltage equations can be written as follows:

$$V_d = R i_d + L \frac{d}{dt} i_d - W_r L i_q \quad (17)$$

$$V_q = R i_q + L \frac{d}{dt} i_q + W_r L i_d + W_r \quad (18)$$

The electromagnetic developed in the machine air gap is given by the following equation:

$$T_e = 1.5P(i_q + (L_d - L_q)i_d i_q) \quad (19)$$

The rotor speed is obtained from the dynamics of the mechanical system as follows:

$$\frac{d}{dt} W_r = \frac{1}{J}(T_e - F W_r - T_M) \quad (20)$$

$$\frac{d}{dt} = W_r \quad (21)$$

The flux equations can be written as follows:

$$= L_d I_d \quad (22)$$

$$_d = i_d L_d + \quad (23)$$

$$_q = i_q L_q \quad (24)$$

where

V_q, V_d are q - and d -axis voltages,

Ψ_d, Ψ_q are flux for d - and q -axis,

L_{qm} is the common q -axis mutual inductance of the stator,

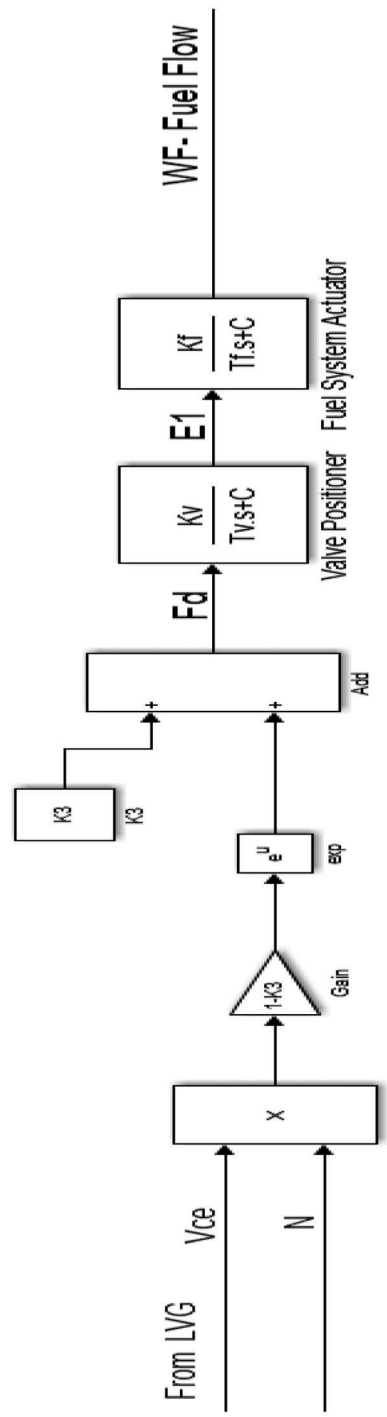


Figure 12. Block diagram of fuel system control.

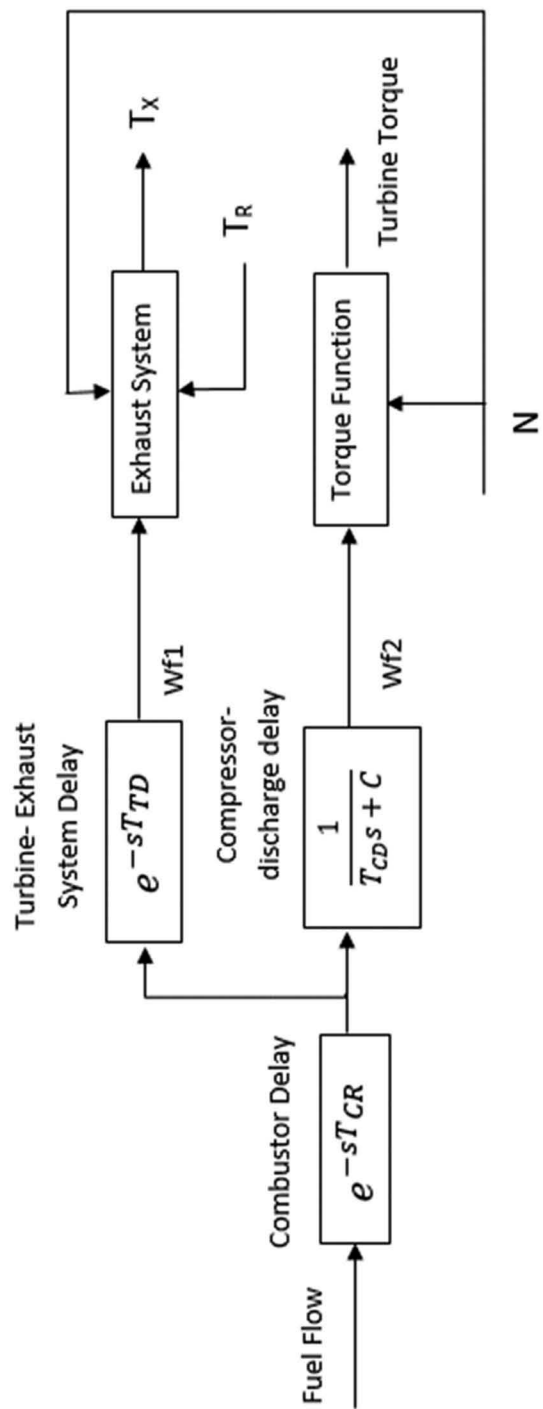


Figure 13. Block diagram of compressor-turbine model.

I_f is the equivalent field current of the permanent magnets,
 F is the viscous friction of rotor and load,
 i_q, i_d are q - and d -axis currents,
 J is the combined inertia of rotor and load,
 L_d, L_q are d - and q -axis inductances,
 P is the number of poles,
 R is the stator windings resistance,
 T_e is the electromagnetic torque,
 T_M is the mechanical torque,
 θ is the angular position of rotor,
 λ is the induced flux in the stator windings, and
 W_r is the rotor angular velocity.

The Simulink model represents the PMSG, as shown in Figure 14.

3.3. Modeling of storage system

The volume of the biogas (methane) required for supplying the load varies according to the load value. A storage system is required to store the excess values of methane gas if any. In the proposed model, the storage system is composed of two parts, a comparator and a storage tank. The comparator compares the volume of methane produced by the reactor with that needed to supply the load. A Simulink model for comparator is shown in Figure 15.

The biogas production per day can be calculated as follows:

$$V_{day} = n * V_b * C_e \quad (25)$$

where

V_{day} is the biogas production per day in Btu/day,
 n is the number of heads of dairy heifers whose manure is fed into a plug-flow anaerobic digester,
 V_b is the biogas production per animal per day in ft³/day,
 C_e is the energy content in Btu/ft³.

The size of generator can be calculated as follows:

$$P_e = V_{day} * \frac{1\text{day}}{24\text{h}} * \eta * \frac{\text{kWh}}{3412\text{Btu}} \quad (26)$$

where:

P_e is the size of generator in kW and
 η is the overall conversion efficiency.

4. Simulink model

A Simulink model for the proposed biogas-fueled power system is developed. The model consists of all the prescribed sub models connected together. In this model, different types of animal manures are fed to the AD as inputs. The generated ac electricity is the model output. In the next sections, the model is implanted for different case studies. However, the model can be divided into two parts: AD model and biogas MT-generation model. Each one of these two models model can be implemented individually to study the impacts of different variables (type of feed, temperature, reactor size ... etc.) on the output of the AD system or to study the impact of methane characteristics on the output of the MT. The proposed biogas MT model is a general one that can be implemented with any other gas type. Figure 16 explains the

complete Simulink model for the proposed biogas-fueled power system.

5. Testing and validation

To verify the proposed model, the model is implemented with the same data used to implement the model described in Pathmasiri, Haugen, and Gunawardena (2013b) and the results are compared. The reactor temperature and volume are taken as 20°C, and 100 m³, respectively. Animal manure (beef) with biodegradable concentration of 0.65 (Kg/m³) is used as a reactor feed. The proposed model is implemented using the above data and the results are graphed in Figure 17(a) whereas the results of the model presented in Pathmasiri, Haugen, and Gunawardena (2013b) are shown in Figure 17(b). The comparison shows the closeness of the results in the two cases. The criteria on which the validation is based are the volume of the produced biogas and the time taken for it to reach its maximum stable value. In the proposed model the maximum value of the biogas volume equals to 132.6 L/day compared to 132.75 L/day for the model in ref. (Pathmasiri, Haugen, and Gunawardena 2013b). Whereas, the time taken for the gas to reach its stable vale is 14 days for the proposed model and 13 days for the model in ref. (Pathmasiri, Haugen, and Gunawardena 2013b).

6. Results and discussion

The proposed model is implemented under different operating conditions in both steady state and transient status to study the impacts of different variables on the system output. The factors required to fully represent the AD process are obtained from experimental analysis given in (Haugen, Bakke, and Lie 2012b) and the MT-PMSG control variables are taken as given in (Guda 2005b). These factors are shown in Appendix 1. Speed reference was kept constant at 1 p.u. for all simulations.

6.1. Steady state operation

In this case, the proposed system is tested for a rated load of 400 kW. The impact of time, feed type and reactor temperature on the AD output is examined and the results are analyzed.

6.1.1. Impact of anaerobic reaction time

In this case, the developed program is implemented to study the change of the cumulative methane production with the anaerobic reaction time. The reactor is fed with diluted animal manure at a fed flow rate of 0.25 m³/day. In this case, the reactor temperature is maintained constant at 35° C as this is the best temperature of bacterial reaction in the AD process (Pathmasiri, Haugen, and Gunawardena 2013b). The results show that, there is a gradually increase in methane production for about 18 days before it becomes constant as shown by Figure 18.

6.1.2. Impact of feed type

The main factor that affects the feed type is the concentration of biodegradable concentration. Table 1 gives the biodegradable concentration for different feed types (Husain 1998b). The proposed model is implemented using different types of

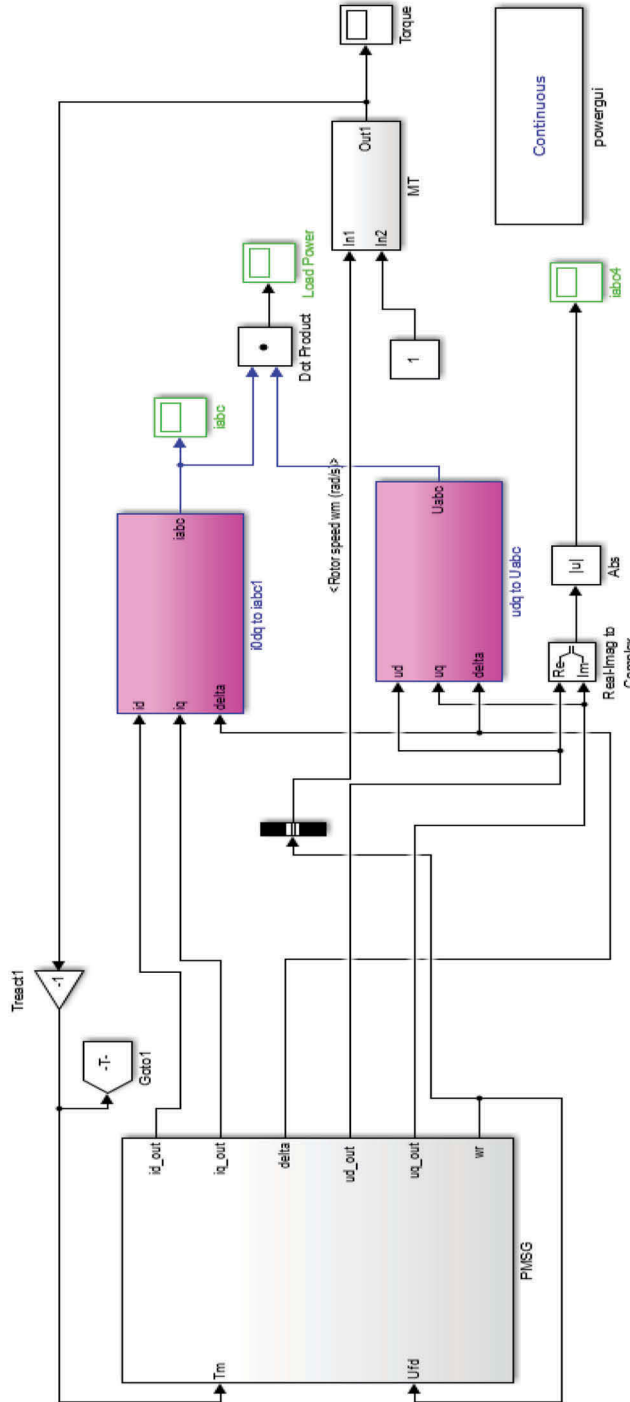


Figure 14. Simulink model for PMSG driven by MT.

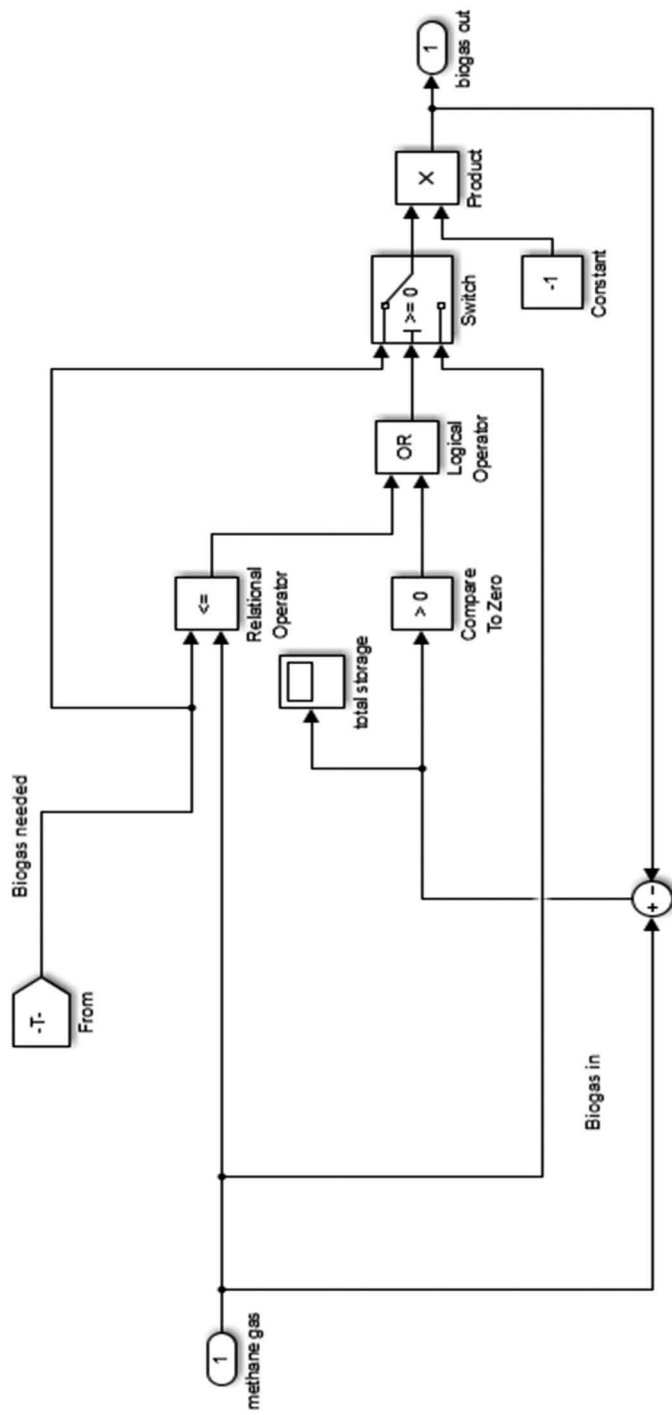


Figure 15. Simulink model for the storage system.

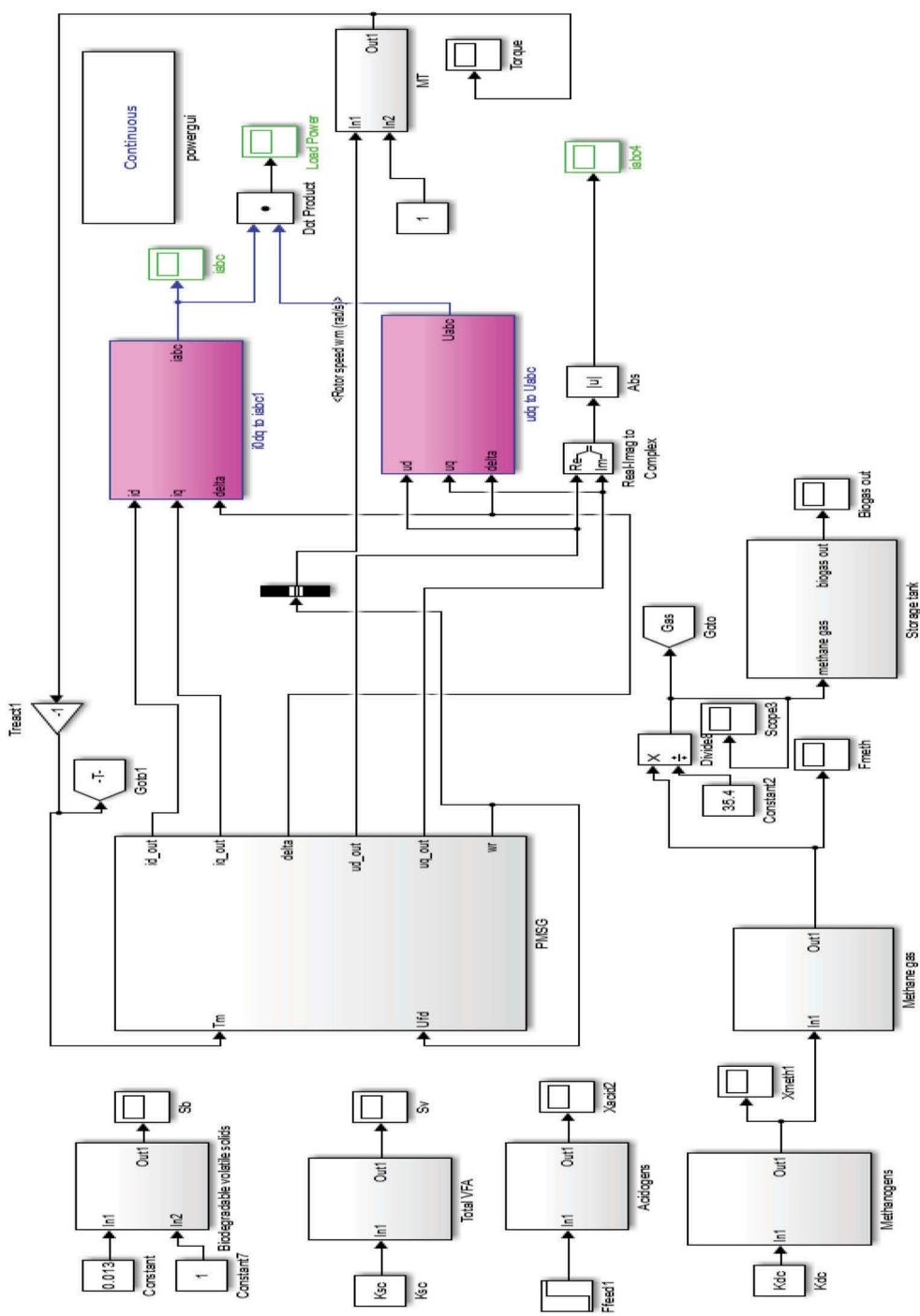


Figure 16. Complete Simulink model for the proposed biogas-fueled power system.

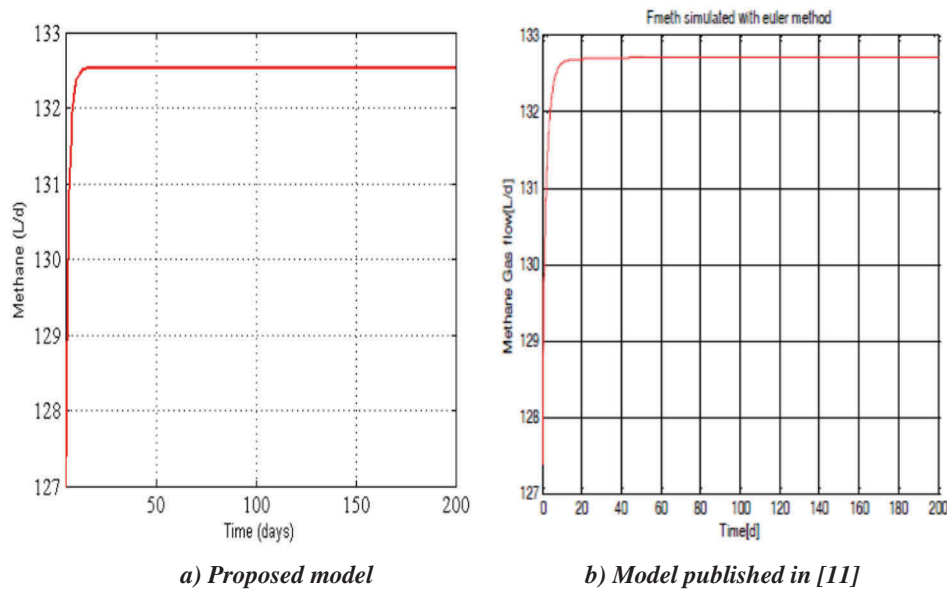


Figure 17. Change of methane with time for the two compared models: (a) proposed model and (b) model published in Pathmasiri, Haugen, and Gunawardena (2013b).

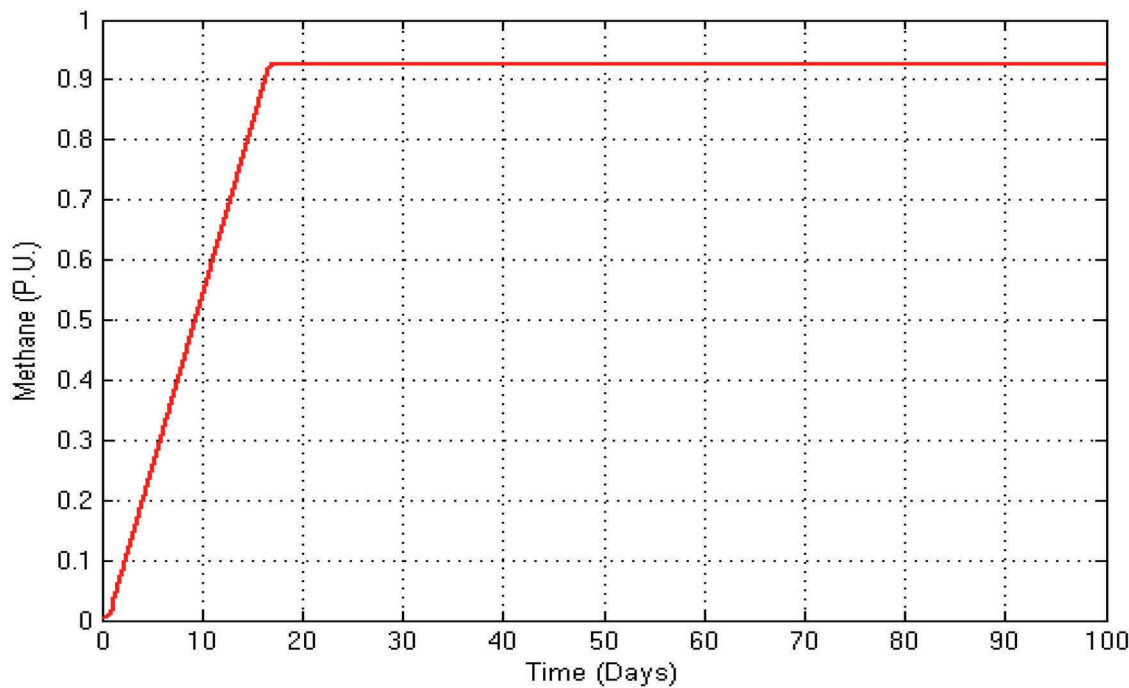


Figure 18. Change of cumulative methane production with anaerobic reaction time (reactor temperature = 35°C).

Table 1. Concentration of biodegradable (Husain 1998b).

Types of feed	Concentration of biodegradable (kg/m ³)
Swine	0.9
Beef	0.65
Poultry	0.7
Dairy manure	0.36

feed and the results is shown in Figure 19. The results show that there is a remarkable change in both methane production period and volume for different feed types. It takes longer period for poultry to reach a constant volume compared to

both swine and beef. The volume of produced methane is decreased heavily when using dairy manure due to its low biodegradable concentration. The outputs are high quality fertilizer produced from filtered solids and biogas consisting of 70–75% methane produced from the liquid fraction of the diluted dairy manure.

6.1.3. Impact of reactor temperature

To discuss the impact of reactor temperature on the methane production, the model is implemented for different reactor

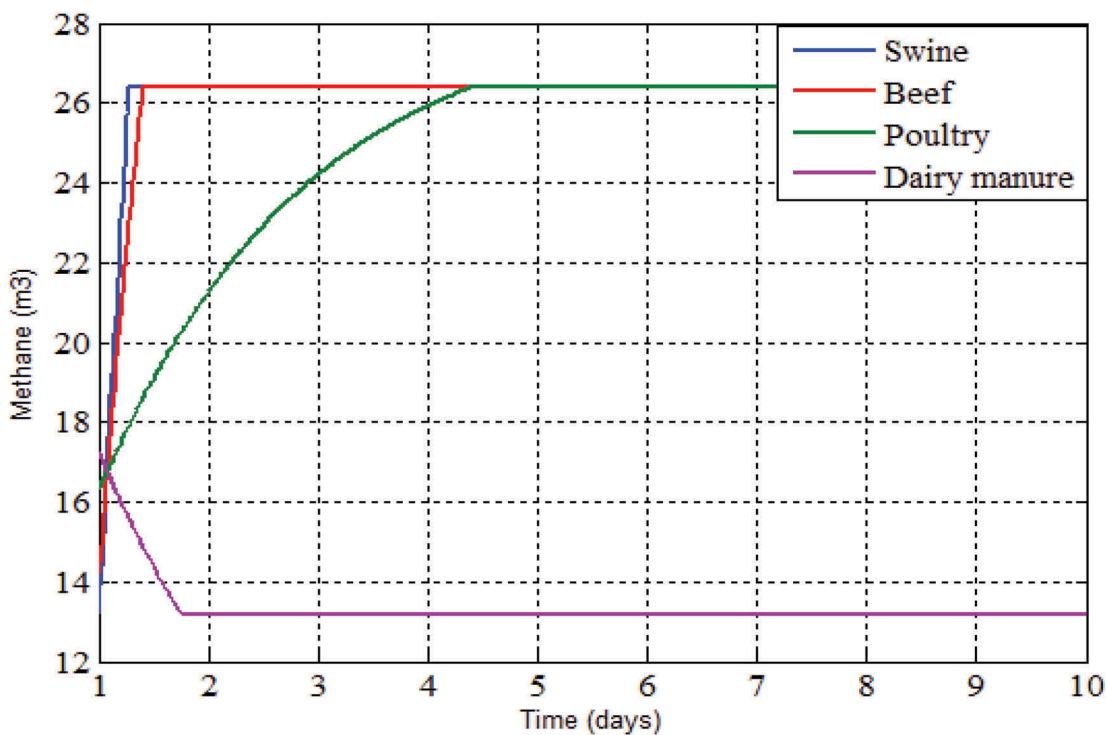


Figure 19. Change of methane production with input feed type.

temperatures. The appropriate temperatures for the fermentation process range from 20 °C to 60 °C (Pathmasiri, Haugen, and Gunawardena 2013b). In case that reactor temperature exceeds than 60 °C, the fermentation process will not complete, because there will be severe reduction in methanogenesis (bacteria) concentration. From the results shown in Figure 20, it can be observed that increasing the reactor temperature leads to an increase in both volume and production period of the methane production. When temperature of reactor is 20 °C the methane out from reactor become to be constant after 52 days, while when temperature of reactor increases methane output from reactor become constant fast as shown in Figure 20.

6.1.4. Variation of output torque during daily biogas production

A dynamic model comprising of four differential equations based on Simulink model for methane gas production was used in this study for the simulation of methane production in an anaerobic digester at the facility. The biogas power plant is mainly composed of a MT connected to some heat exchangers in a regenerative Brayton cycle using clean air as process fluid. The usual burners of the standard MTs are replaced by a high temperature heat exchanger for heating the process air from the biogas combustion. Biogas is supplied to the heat generator through a screw conveyor, which is suitable to drive the biogas in the lowest zone of the combustion chamber. Different options have been used for storing and conveying the biogas. The combustion air and process air are fully

decoupled. The process air is pressurized by a centrifugal compressor, directly connected to the turbine shaft, and forced into the regenerative heat exchanger before flowing in the high temperature heat exchanger inside the biogas fired heat generator. After crossing the turbine, the expanded, but still hot, air flows into the regenerative heat exchanger (recuperator) for warming the compressed clean air.

External air enters both in the micro-turbine and in the heat generator and the exhaust flow is the sum of these two contributions. The output air is then mixed with the combustion exhausts to be directly used for thermal applications, or to warm some water (either pressurized or not) which, in turns, can be exploited for thermal use or to supply an Organic Rankine cycle.

The produced methane is used to create the required load torque in the MT. Figure 21 shows the variations of MT output torque with time. The torque increases with increasing the methane production until it reaches a rated value as the methane production becomes constant. According to torque profile shown in Figure 21, it is recommended that, the reactor has to run for sufficient days before it is connected to the electrical system for supplying a specified load.

6.2. Transient operation

To prove the robustness of the model, the proposed model is implemented in transient conditions, i.e., sudden load changes (increase and/or decrease). The load is assumed to be increased to 200 kW at day 70, then to 300 kW at day 80,

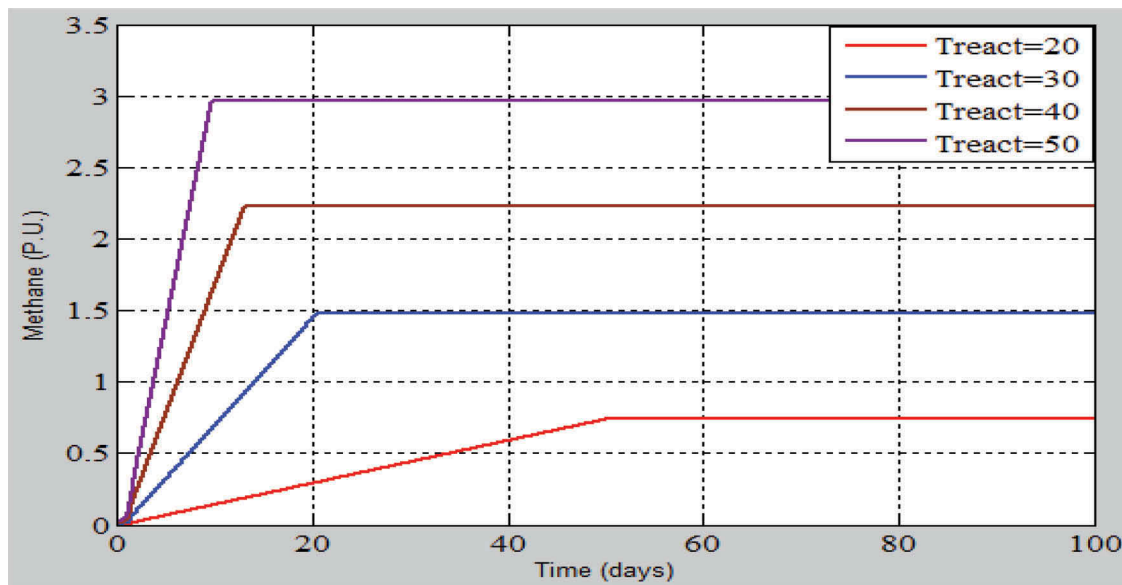


Figure 20. Variation of methane production with reactor temperature.

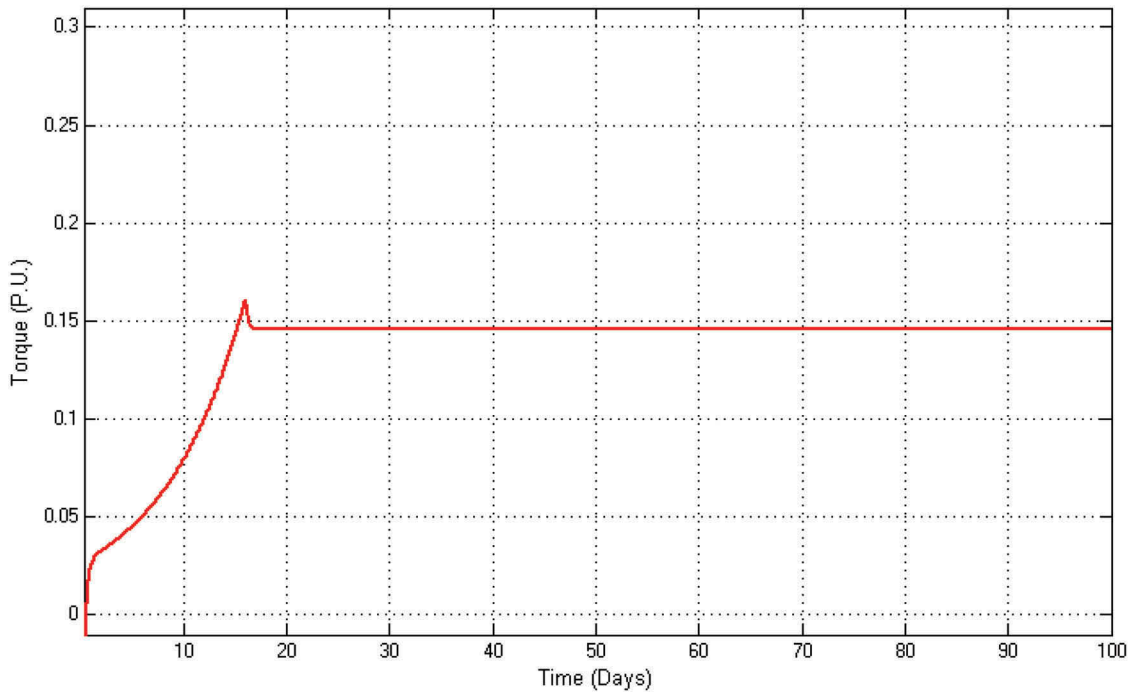


Figure 21. MT output torque during daily biogas production.

and finally it is decreased to 250 kW at day 90. The impact of these changes on both MT torque, generator speed and storage system are studied.

6.2.1. Impact of load variations on MT torque

Figure 22 shows the impact of load variations on MT torque. Firstly, the torque is increased by increasing the volume of the produced methane. When the methane reaches a constant volume, the torque decreases to match the load. It is shown that, as the load increases at days 70 and 80, the torque is increased to 0.148 and 0.154 p.u., respectively. As the load decreases at day 90, the torque is decreased to be 0.152 p.u.

These results show that the proposed model works properly as the torque changes with any change in load.

6.2.2. Impact of load variations on generator speed

Figure 23 shows the impact of load changes on the generator speed. The speed decreases with load increase (at days 70 and 80) and increases with load decrease (at day 90) which improves the robustness of the model.

6.2.3. Impact of load variations on storage system

The amount of methane stored in the tank decreases by increasing the load at days 70 and 80 and increases by decreasing load

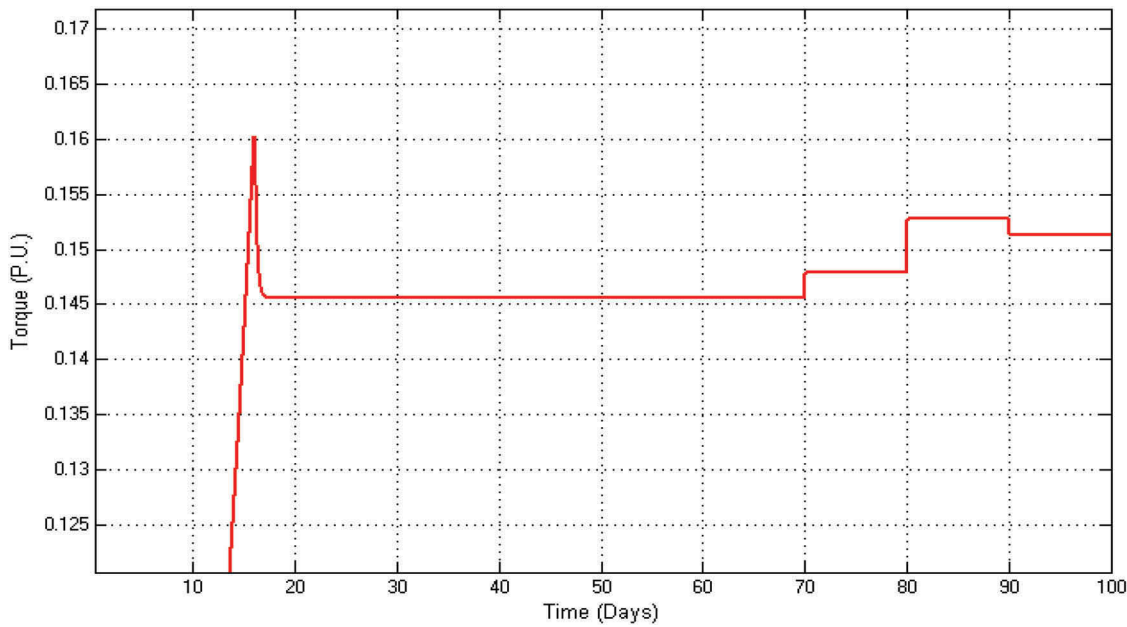


Figure 22. Variation of MT torque with load changes.

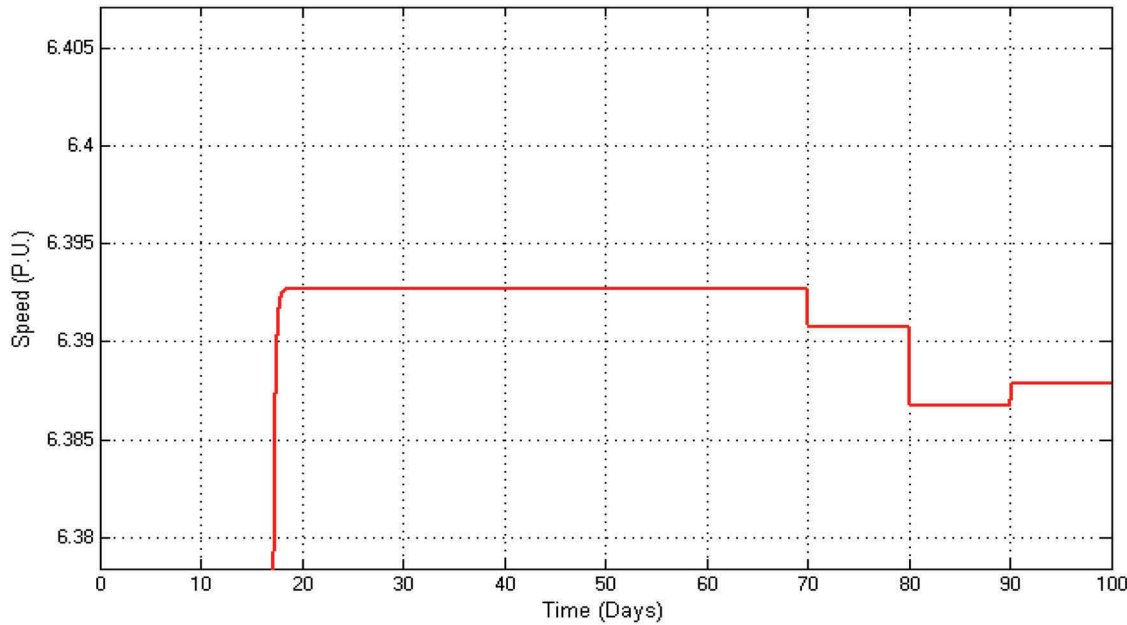


Figure 23. Variation generator speed with load changes.

at day 90 as explained by [Figure 24](#). The results prove that the storage system model works properly.

[Figures 22–24](#) show that the proposed model works effectively. As the load changes (increase and decrease), the torque is also changes. The volume of methane stored in the storage system decreases by increasing the load and increases by decreasing load and the speed of generator is also decreased by increasing load and increased by decreasing load.

7. Conclusion

This paper presents a detailed Modeling and simulation of a biogas-fueled power system. The proposed model is composed of three individual models represent a biogas reactor, an MT-generation system and a storage system. Based on the specific requirements, each model can be implemented individually or collectively to simulate the biogas power plant. The model describes the dynamics of an MT and it is suitable for both steady

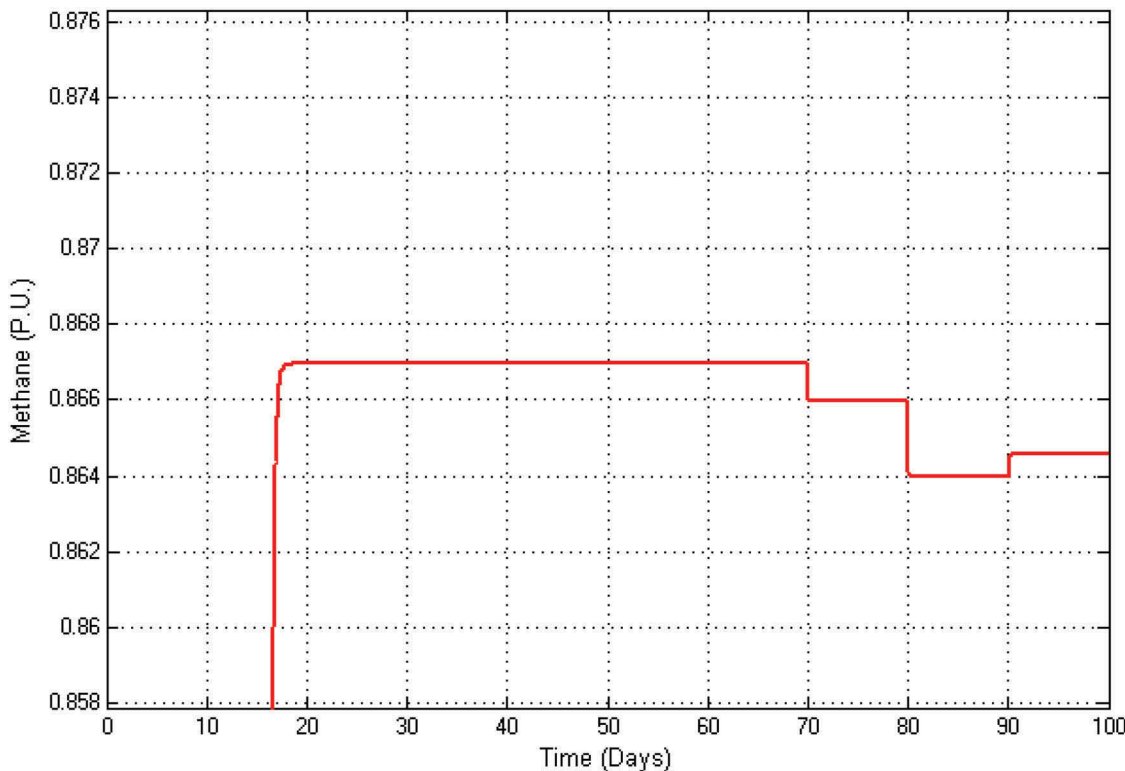


Figure 24. Variation of stored methane with load changes.

state and transient simulation and analysis. An adaptive controller was developed to withstand the plant against any transient condition. The model was implemented and tested in Matlab/Simulink environment. The impact of time, feed type and reactor temperature on the AD output was examined and the results were analyzed. Different operating conditions in both steady state and transient status were investigated to study the impacts of these variables on the system output. The simulation results proved the role of the proposed system as a reliable power source and its robustness and effectiveness for different sudden load changes. For all operating conditions, the MT succeeded to feed the generator load either from the biogas reactor directly or from the storage tank. The performance of the proposed model verified its applicability and effectiveness under different operating conditions as it assesses all the power plant operating variables.

Highlights

- A Simulink model for biogas power plant using micro-turbine is proposed.
- Each part in the proposed model can be studied and simulated separately.
- The proposed model is fueled with biogas produced from Anaerobic Digestion (AD) process of the diluted animal manure.
- The proposed model studied the four steps of Anaerobic Digestion (AD) process.
- The proposed model used the microturbine (MT) to generate electricity which is small gas turbine.
- The proposed model studied at normal and transient operation.

- The response of the proposed model at transient operation is efficient and fast

References

- Abdollahi, S. E., and A. Vahedi. 2005b. Dynamic modelling of micro-turbine generation systems using Matlab/Simulink. *Renewable Energy and Power Quality Journal* 1:146–52. doi:[10.24084/repqj03.243](https://doi.org/10.24084/repqj03.243).
- Al-Hinai, A., and A. Feliachi. 2002b. Dynamic model of a microturbine used as a distributed generator. Proceedings of the Thirty-Fourth Southeastern Symposium on System Theory, 209–13. doi: [10.1109/SSST.2002.1027036](https://doi.org/10.1109/SSST.2002.1027036).
- Asgharian, P., and R. Noroozian. 2016b. Modelling and simulation of microturbine generation system for simultaneous grid-connected/islanding operation. Iranian Conference on Electrical Engineering. doi: [10.1109/IranianCEE.2016.7585764](https://doi.org/10.1109/IranianCEE.2016.7585764).
- Barsali, S., A. D. Marco, R. Giglioli, G. Ludovici, and A. Possenti. 2015b. Dynamic modelling of biomass power plant using micro gas turbine. *Renewable Energy* 80:806–18. doi:[10.1016/j.renene.2015.02.064](https://doi.org/10.1016/j.renene.2015.02.064).
- Capareda, S. 2013b. *Introduction to biomass energy conversions*. Book. CRC Press, USA.
- Corigliano, O., G. Florio, and P. Fragiocomo. 2012b. A numerical simulation model of high temperature fuel cells fed by biogas. *Energy Sources, Part A: Recovery, Utilization, and Environmental Effects* 34:101–10. doi:[10.1080/15567036.2011.584116](https://doi.org/10.1080/15567036.2011.584116).
- De Lorenzo, O., C. M. Lo Faro, P. Frontera, P. Antonucci, S. C. Zignani, S. Trocino, F. A. Mirandola, A. S. Aricò, and P. Fragiocomo. 2016b. Thermoelectric characterization of an intermediate temperature solid oxide fuel cell system directly fed by dry biogas. *Energy Conversion and Management* 127:90–102. doi:[10.1016/j.enconman.2016.08.079](https://doi.org/10.1016/j.enconman.2016.08.079).
- Duan, Z., M. N. C. Bournazou, and C. Kravaris. 2017b. Dynamic model reduction for two-stage anaerobic digestion processes. *Chemical Engineering Journal* 1–49. doi:[10.1016/j.cej.2017.06.110](https://doi.org/10.1016/j.cej.2017.06.110).
- Galvagno, A., V. Chiodo, F. Urbani, and F. Freni. 2013b. Biogas as hydrogen source for fuel cell applications. *International Journal of Hydrogen Energy* 38:3913–20. doi:[10.1016/j.ijhydene.2013.01.083](https://doi.org/10.1016/j.ijhydene.2013.01.083).

- Guda, S. 2005b. Modelling and power management of a hybrid wind microturbine power generation system. MSc diss., Montana State University.
- Guda, S., C. Wang, and M. H. Nehrir. 2006b. Modelling of microturbine power generation systems. *Electric Power Components and Systems* 1027–41. doi:10.1080/15325000600596767.
- Hagos, K., J. Zong, D. Li, C. Liu, and X. Lu. 2017b. Anaerobic co-digestion process for biogas production: Progress, challenges and perspectives. *Renewable and Sustainable Energy Reviews* 76:1485–96. doi:10.1016/j.rser.2016.11.184.
- Haugen, F., R. Bakke, and B. Lie. 2012b. *Mathematical modelling for planning optimal operation of a biogas reactor for dairy manure*. Dublin: IWA World Congress on Water, Climate and Energy. May. 14–18.
- Husain, A. 1998b. Mathematical models of the kinetics of anaerobic digestion- A selected review. *Biomass and Bioenergy* 14:561–71. doi:10.1016/S0961-9534(97)10047-2.
- Jurado, F., M. Ortega, A. Cano, and J. Carpio. 2002b. Neuro-fuzzy controller for gas turbine in biomass-based electric power plant. *Electric Power Systems Research* 123–35. doi:10.1016/S0378-7796(01)00187-0.
- Khorshidi, A., M. Zolfaghari, and M. Akhavan. 2014b. Dynamic modelling and simulation of microturbine generating system for stability analysis in microgrid networks. *International Journal of Basic Sciences & Applied Research* 3:663–70. <http://www.isicenter.org>.
- Liao, Q., J. Chang, C. Herrmann, and A. Xia. 2018b. *Bioreactors for microbial biomass and energy conversion book*. Springer. doi:10.1007/978-981-10-7677-0.
- Manjusha, C., and S. Beevi. 2016b. Mathematical modelling and simulation of anaerobic digestion of solid waste. *Procedia Technology* 24:654–60. doi:10.1016/j.protcy.2016.05.174.
- McKendry, P. 2002c. Energy production from biomass (part 1): Overview of biomass. *Bioresource Technology* 83:37–46. doi:10.1016/S0960-8524(01)00118-3.
- McKendry, P. 2002d. Energy production from biomass (part 2): Conversion technologies. *Bioresource Technology* 83:47–54. doi:10.1016/S0960-8524(01)00119-5.
- Neshata, S. A. S., M. Mohammadia, G. D. Najafpoura, and P. Lahijani. 2017b. Anaerobic co-digestion of animal manures and lignocellulosic residues as a potent approach for sustainable biogas production. *Renewable and Sustainable Energy Reviews* 79:308–22. doi:10.1016/j.rser.2017.05.137.
- Pathmasiri, T., F. Haugen, and S. H. P. Gunawardena. 2013b. Simulation of a biogas reactor for dairy manure. *Annual Transactions of IESL* Vol. 1, Part B, 394–98.
- Rathnasiri, P. G. 2016b. Dynamic modelling and simulation of pilot scale anaerobic digestion plant treating source separated food waste and effect of recycling sludge. *Procedia Environmental Sciences* 35:740–48. doi:10.1016/j.proenv.2016.07.082.
- Saroj. 2012b. Simulink model of biomass. MSc diss., California State University.
- Shi, X.-S. X.-S., X. Yuan, Y. Wanga, S. Zeng, Y. Qiu, R. Guo, and L. Wanga. 2014b. Modelling of the methane production and PH value during the anaerobic co-digestion of dairy manure and spent mushroom substrate. *Chemical Engineering Journal* 244:258–63. doi:10.1016/j.cej.2014.02.007.
- Ting Chen, D., S. Y. Jin, H. Li, Z. Yu, H. Feng, Y. Long, and J. Yin. 2017b. Comprehensive evaluation of environ-economic benefits of anaerobic digestion technology in an integrated food waste-based methane plant using a fuzzy mathematical model. *Applied Energy*. 1–12. doi:10.1016/j.apenergy.2017.09.082.
- Weinrich, S., and M. Nelles. 2015b. Critical comparison of different model structures for the applied simulation of the anaerobic digestion of agricultural energy crops. *Bioresource Technology* 178:306–12. doi:10.1016/j.biortech.2014.10.138.
- Wellinger, A., J. Murphy, and D. Baxter. 2013b. *The biogas handbook book*. Wood head Publishing Limited. doi:10.1533/9780857097415.1.
- Zhang, Q., J. Hu, and D. Lee. 2016b. Biogas from anaerobic digestion processes: Research updates. *Renewable Energy* 98:108–19. doi:10.1016/j.renene.2016.02.029.

Appendix 1. Factors and parameters used in the proposed model (Guda 2005b, Haugen, Bakke, and Lie 2012b, Pathmasiri, Haugen, and Gunawardena 2013b)

	AD	MT
B	4.91	25
K_s	21.5 kg/m ³	0.8
K_{sc}	3 kg/m ³	0.2
K_d	0.02 d ⁻¹	0.4
K_{dc}	0.02 d ⁻¹	1
K_1	9.66	15
K_2	6.97	2.5
K_3	31.8	3.3
K_4	15.1	450 °F
X_{meth}	0.35 kg /m ³	3
X_{acid}	1.20 kg /m ³	1
Sb_{in}	13.8 kg /m ³	0.05
Sb	4.51 kg /m ³	1
Sv_{in}	2.91 kg /m ³	0.23
Sv	0.63 kg /m ³	1
V	20 m ³	950 °F
PMSG		
R	12.5 Ω	0.04
L_d	165e-6 H	0.01
L_q	165e-6 H	0.04
W_r	70000 rpm	0.2
P	4 poles	KH
J	0.011 kgm ²	1.2
λ	0.2388 wb	

Appendix 2. Equations describe the compressor-turbine model (Jurado et al. 2002b)

$$P_c = \frac{W_a h_{IC}}{\eta_c \eta_{trans}} \quad (a.1)$$

$$W_g C_{pg} (T_{Tin} - 298) + W_f h + W_a C_{pa} (298 - T_{cout}) + W_{is} C_{ps} (298 - T_{is}) = 0 \quad (a.2)$$

$$P_T = \eta_T W_g h_{IT} \quad (a.3)$$

$$P_{mec} = P_T - P_c \quad (a.4)$$

where

P_c	Compressor power consumption
W_a	Air mass flow into the compressor
Δh_{IC}	Isentropic enthalpy change for a compression from P_{cin} to P_{cout}
η_c	Overall compressor efficiency
η_{trans}	Transmission efficiency from turbine to compressor
C_{pg}	Specific heat of combustion gases
C_{pa}	Specific heat of air at constant pressure
C_{ps}	Specific heat of steam
W_g	Turbine gas mass flow
T_{Tin}	Turbine inlet gas temperature
W_f	Fuel mass flow
T_{is}	Temperature of injected steam
W_{is}	Injection steam mass flow
Δh	Specific enthalpy of reaction at reference temperature
Δh_{IT}	Isentropic enthalpy change for a gas expansion from P_{Tin} to P_{Tout}
η_T	Overall turbine efficiency
P_{mec}	Mechanical power delivered by turbine
P_T	Total mechanical power delivered by turbine

Appendix 3. Simulink model of MT including all its control systems

